

A. Huber, G. Arnoux, S.A. Bozhenkov, S. Brezinsek, C. Fuchs, W. Fundamenski,
S. Jachmich, U. Kruezi, M. Lehnen, A. Loarte, G.F. Matthews, Ph. Mertens,
V. Philipps, R.A. Pitts, U. Samm, B. Schweer, G. Sergienko, M. Stamp
and JET EFDA contributors

Radiation Heat Loads on Plasma-Facing Components of JET during the Massive Gas Injection Experiment

Radiation Heat Loads on Plasma-Facing Components of JET during the Massive Gas Injection Experiment

A. Huber¹, G. Arnoux², S.A. Bozhenkov¹, S. Brezinsek¹, C. Fuchs³, W. Fundamenski²,
S. Jachmich⁴, U. Kruezi¹, M. Lehnen¹, A. Loarte⁵, G.F. Matthews², Ph. Mertens¹,
V. Philipps¹, R.A. Pitts⁵, U. Samm¹, B. Schweer¹, G. Sergienko¹, M. Stamp²
and JET EFDA contributors*

JET-EFDA, Culham Science Centre, OX14 3DB, Abingdon, UK

¹*Institute of Energy and Climate Research - Plasma Physics, Forschungszentrum Jülich GmbH,
Association EURATOM-FZJ, Partner In the Trilateral Euregio Cluster, Jülich, Germany*

²*EURATOM-CCFE Fusion Association, Culham Science Centre, OX14 3DB, Abingdon, OXON, UK*

³*Max-Planck-Institut für Plasmaphysik, EURATOM Association, D- 85748 Garching, Germany*

⁴*Laboratory for Plasma Physics, ERM/KMS, Association EURATOM-Belgian State,
B-1000 Brussels, Belgium*

⁵*ITER Organization, Cadarache, France*

** See annex of F. Romanelli et al, "Overview of JET Results",
(23rd IAEA Fusion Energy Conference, Daejeon, Republic of Korea (2010)).*

Preprint of Paper to be submitted for publication in Proceedings of the
38th EPS Conference on Plasma Physics
Strasbourg, France
(27th June 2011 - 1st July 2011)

“This document is intended for publication in the open literature. It is made available on the understanding that it may not be further circulated and extracts or references may not be published prior to publication of the original when applicable, or without the consent of the Publications Officer, EFDA, Culham Science Centre, Abingdon, Oxon, OX14 3DB, UK.”

“Enquiries about Copyright and reproduction should be addressed to the Publications Officer, EFDA, Culham Science Centre, Abingdon, Oxon, OX14 3DB, UK.”

The contents of this preprint and all other JET EFDA Preprints and Conference Papers are available to view online free at www.iop.org/Jet. This site has full search facilities and e-mail alert options. The diagrams contained within the PDFs on this site are hyperlinked from the year 1996 onwards.

INTRODUCTION

During plasma disruptions in JET, the thermal energy ($\leq 10\text{MJ}$) and magnetic energy ($\leq 20\text{MJ}$) are lost in the form of heat to the plasma-facing components (PFC) on time scales of less than 1ms and 20ms [1], respectively. The thermal energy W_{th} stored in the plasma is dissipated initially in the thermal quench (TQ), followed by the magnetic energy dissipation in the current quench (CQ). During the thermal quench phase of the unmitigated disruptions the main part of the thermal energy is lost by convection to the first wall and only a small part ($\leq 0.2 \times W_{\text{th}}$) by radiation [2]. The energy deposition is distributed non-uniformly over the first wall surfaces and it may significantly contribute to the local power loads onto PFCs.

RESULTS AND DISCUSSION

The conducted/convected heat loads during the TQ-phase can be reduced by enhancing the radiation with Massive Gas Injection (MGI). For investigation of the radiation behaviour, a tomographic reconstruction model is used (anisotropic diffusion model) that has been coupled with a Monte-Carlo technique to calculate the radiation heat flux onto the wall and the corresponding ‘‘Radiation Peaking Factor’’ (RPF) (the local radiation power load onto the wall is normalised to its value averaged over the entire surface). The method delivers the radiation power load with a temporal resolution of $\sim 1\text{ms}$ in a 2D-poloidal plane and it has been mapped to the entire surface assuming toroidal symmetry.

A fast valve (Disruption Mitigation Valve-DMV) has recently been installed at JET to study the disruption mitigation by massive gas injections [3]. The valve is positioned on top of the machine and the gas is guided by a 4m long tube to the plasma. Different gas species have been investigated: Ne, Ar, He, mixtures of Ne and Ar with 90% of D_2 and pure D_2 . Figure 1 shows the selection of key plasma parameters of a typical induced JET disruption caused by an injection of a mixture of 10%Ar with 90% D_2 into NBI heated plasma: $P_{\text{NBI}} = 9\text{MW}$, $B_{\text{T}} = 3\text{T}$, $I_{\text{p}} = 2.0\text{MA}$, thermal energy of $W_{\text{th}} = 3.2\text{MJ}$ and the magnetic energy of $W_{\text{mag}} = 10.5\text{MJ}$. About 5×10^{21} Argon atoms have been injected into the main chamber. After the activation of the DMV, the gas flows through the tube and arrives at the plasma edge with a delay of 2ms. At that time the cooling of the plasma edge starts triggering the reduction of the plasma thermal energy. In the precursor phase, up to 95% ($\Delta W_{\text{th}} \approx 1.05\text{MJ}$, $E_{\text{rad}} \approx 1.0\text{MJ}$) of the thermal energy is lost predominantly by radiation before the TQ. About 97% ($\Delta W_{\text{th}} \approx 2.15\text{MJ}$, $E_{\text{rad}} \approx 2.1\text{MJ}$) of the remaining energy is radiated during the TQ. Here we used the definition for the end of the thermal quench the time where SXR emission is reduced to noise level [4]. This is consistent with earlier JET result of 90-100% of radiation fraction during massive gas injections of gas mixtures with deuterium (10%Ar or 10%Ne with 90% D_2) reported in [4]. The analysis by divertor thermography shows that only about 5% of W_{th} is found in the (outer) divertor [5] confirming the high radiation fraction. Additionally Fig.1 shows the tomographic reconstruction of the radiation at three different times: at the end of the precursor and TQ phases, and during the CQ-phase. The radiated power shows a very homogenous poloidal distribution with

a peaking factor below 1.5 as shown in Fig.2 during the thermal and current quench. In contrast, a peaking factor of 3.5 is found during the TQ in an unmitigated VDE, which could increase the Be temperature in ITER to values around 40% of the melting point [2]. These “peaking factors” have been used to extrapolate to ITER reference conditions. The ‘ablation/melting parameter’ [1], which determines the surface temperature rise caused by disruption during TQ phase, can reach in ITER a value of $13\text{MJm}^2\text{s}^{-1/2}$. It was assumed here that 50% of the initial thermal energy ($W_{\text{th}} = 350\text{MJ}$) is deteriorated just during the precursor phase without significant increase of the wall surface temperature and the remaining plasma energy of $1/2 \times W_{\text{th}} = 175\text{MJ}$ is completely lost by the radiation with $\text{RPF} = 1.5$ during $t_{\text{tq}} \approx 1\text{ms}$ of TQ phase. This is below the Be melting limit of about $20\text{MJm}^{-2}\text{s}^{-1/2}$. In MGI disruptions, strong localised radiation and larger poloidal peaking of up to 2.5 is observed at the beginning of the cooling phase when the first gas arrives at the plasma. The risk to melt Be by local radiation heat load is of concern for ITER. Fig.3 shows the time resolved RPF factors for the precursor phase. More than half of the time of the cooling phase the radiation is strongly localised at the injection port with large poloidal factors $\text{RPF} = 2.5$. At the beginning of the cooling phase the radiation can also have strong toroidal asymmetry. In [4] the toroidal RPF has been estimated from the visible emission recorded by fast camera during the gas injection. This emission does not contain the emission from the ions with higher degree of ionization and correspondingly do not reflect the behaviour of the total radiation. But it will give the upper limit of the Toroidal Peaking Factor (TPF). Thus, assuming this worse case with toroidal $\text{RPF} = 5-8$ [4] and poloidal $\text{RPF} = 2.5$ for the first 4ms of the cooling phase in ITER, we will find a ‘melting parameter’ of $50-80\text{MJm}^{-2}\text{s}^{-1/2}$. This is factor 4 more than the threshold for Be melting. The melting can be avoided by the application of at least 4 injection ports in ITER.

A combined VDE+MGI experiment was performed to demonstrate the efficiency of the MGI technique after the loss of control of the vertical plasma position. In this experiment, the upward VDE was triggered by the vertical stabilisation system of JET. The Fig.4 shows the comparison between pure VDE and VDE-MGI experiments with similar plasma parameters before MGI activation: $I_p = 1.5\text{MA}$, $B_T = 1.85\text{T}$, $q_{95} = 3.7$. The direct comparison of the surface temperature on the upper dump plate shows the factor of 2 larger temperature rise in the case of pure VDE experiment. After about 14ms of the VDE triggering (MGI was activated after 10ms of VDE triggering), the cooling phase with MGI started. The observed RPF in VDE+MGI experiment was 2.14, compared to 3.5 for pure VDE experiment (without MGI), and 1.5 for pure MGI disruption (without VDE). In contrast to JET the VDEs in ITER will take place on the longer timescale of $\sim 1\text{s}$ and we expect that the radiation behaves like in the pure MGI experiment. Considering the $\text{RPF} = 2.14$, the ‘ablation/melting parameter’ in ITER would be $\sim 17\text{MJm}^{-2}\text{s}^{-1/2}$ corresponding to the increase of the Be surface temperature to values below the melting point. Thus the combined experiment shows that the $\text{RPF} = 2.14$ is much smaller than the peaking factor during the precursor and TQ in a pure VDE disruption, demonstrating the feasibility of the MGI technique even after a loss of control of the vertical plasma position. During the CQ, like in pure MGI experiment as well in unmitigated

disruption (see Fig.4c), the significant part of the W_{mag} (about 45%) was converted in radiation and spread nearly uniformly over the walls. Assuming $W_{\text{mag}}=395\text{MJ}$ inside the vessel, time of current quenches of $t_{\text{CQ}} = 37\text{ms}$, poloidal RPF=2.14, the ‘ablation/melting parameter’ in ITER would be $\sim 6\text{MJm}^{-2}\text{s}^{-1/2}$ that is a factor of 3 beyond the melting of the Be. Thus, radiation load during the CQ is not a critical issue even for the unmitigated disruptions.

SUMMARY AND CONCLUSIONS

- Unmitigated disruptions exhibit small radiation fractions during precursor and TQ with strong poloidal asymmetry distribution.
- More than 90% of W_{th} and a significant part of W_{mag} was converted in radiation and spread uniformly over the walls. By divertor thermography, only about 5% of W_{th} is found in the (outer) divertor
- Nearly symmetric poloidal distributions of the radiation during precursor, thermal and current quenches have been observed (RPFs ≤ 1.5).
- The radiation is strongly localised at the beginning of the gas injection. The Be melting limit of about $20\text{MJ m}^{-2}\text{s}^{-0.5}$ suggests the use of at least 4 injection ports in ITER.
- The plasma radiation analysis during the combined VDE + MGI experiments shows a slight reduction of the radiation poloidal symmetry (maximum of RPF of 2.14 to be compared to 1.5) in comparison with pure MGI experiment.
- About 70-80% of W_{th} are radiated during the precursor and TQ phases

ACKNOWLEDGEMENT

This work, supported by the European Communities under the contract of Association between EURATOM and FZJ, was carried out within the framework of the European Fusion Development Agreement. The views and opinions expressed herein do not necessarily reflect those of the European Commission.

REFERENCES

- [1]. V. Riccardo et al., Nuclear Fusion **45** (2005) 1427
- [2]. A. Huber et al., accepted for publication in Journal of Nuclear Materials
<http://dx.doi.org/10.1016/j.jnucmat.2010.10.061>
- [3]. U. Kruezi et al., 36th EPS Conference on Plasma Physics Sofia, 2009 ECA Vol.33E, P-2.153 (2009)
- [4]. M. Lehnen et al 23rd IAEA 2010 EXS/P2-13
- [5]. G. Arnoux et al., accepted for publication in Nuclear Materials
[doi:10.1016/j.jnucmat.2010.11.042](http://dx.doi.org/10.1016/j.jnucmat.2010.11.042)

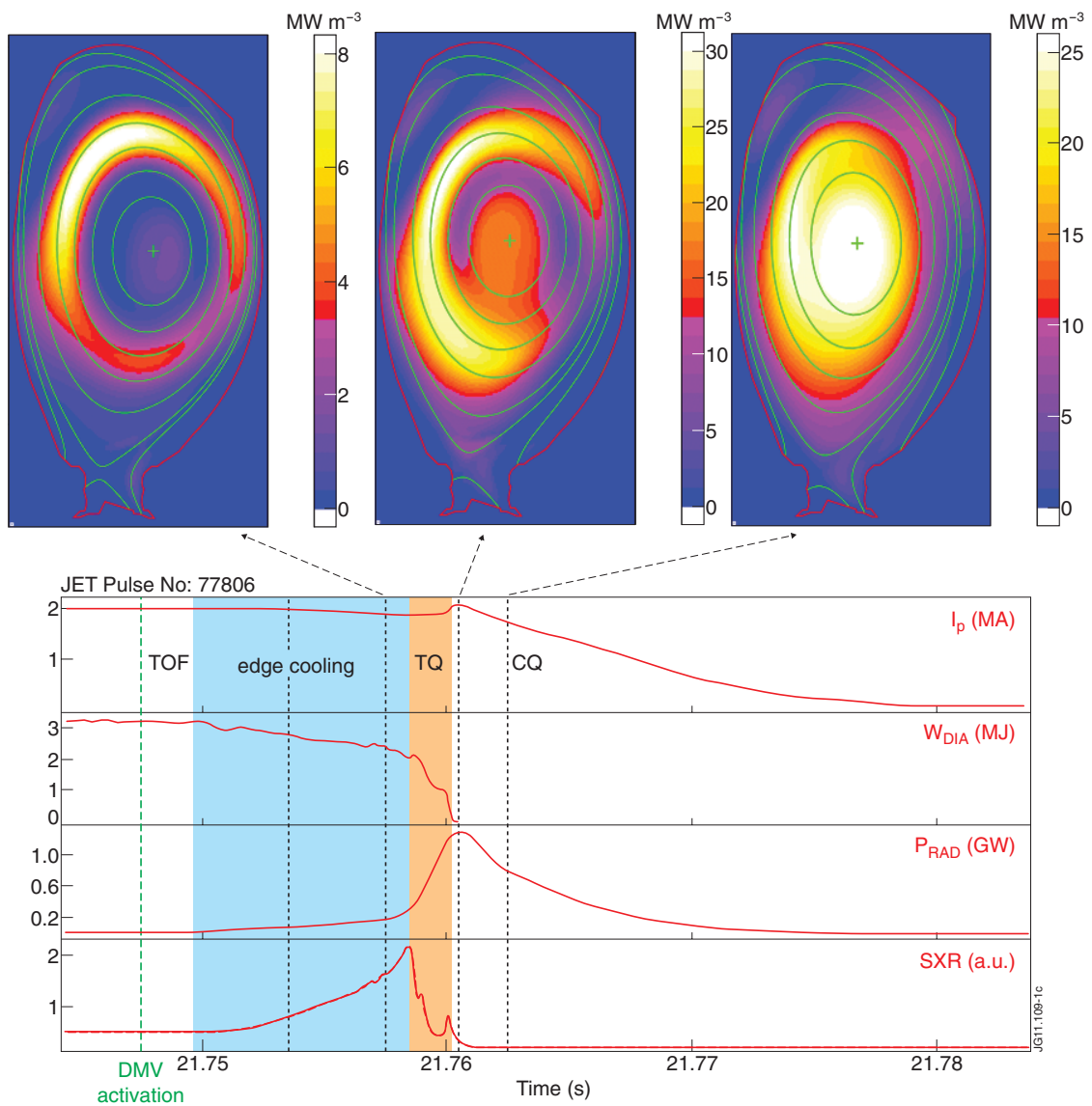


Figure 1: Time traces during a typical induced disruption caused by injection of a mixture of 10%Ar and 90% D₂. Also shown are the radiation distributions during different time phases of the disruption.

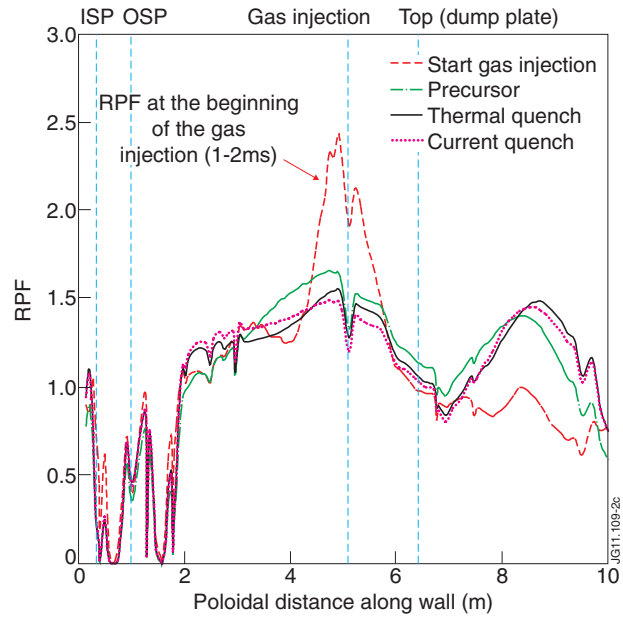


Figure 2: Radiation peaking factors during the different phases of the MGI experiment discussed in Figure 1.

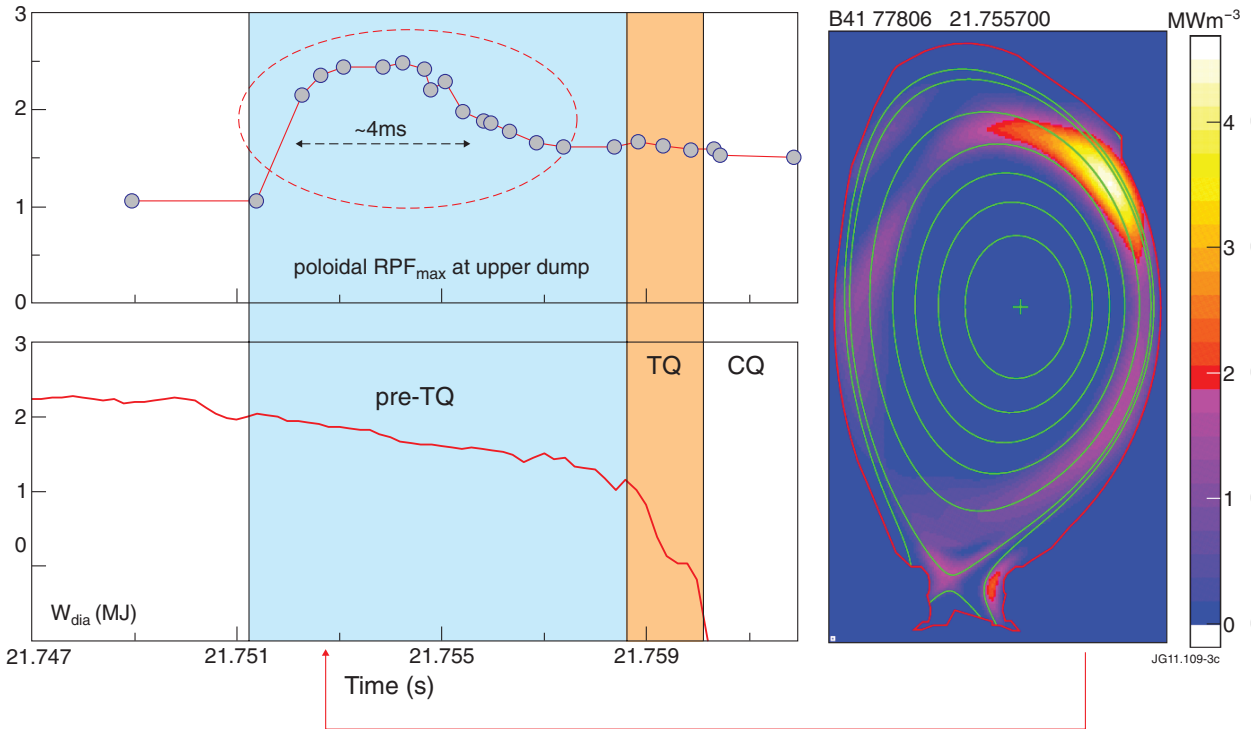


Figure 3: Time resolved RPF factors during the precursor phase.

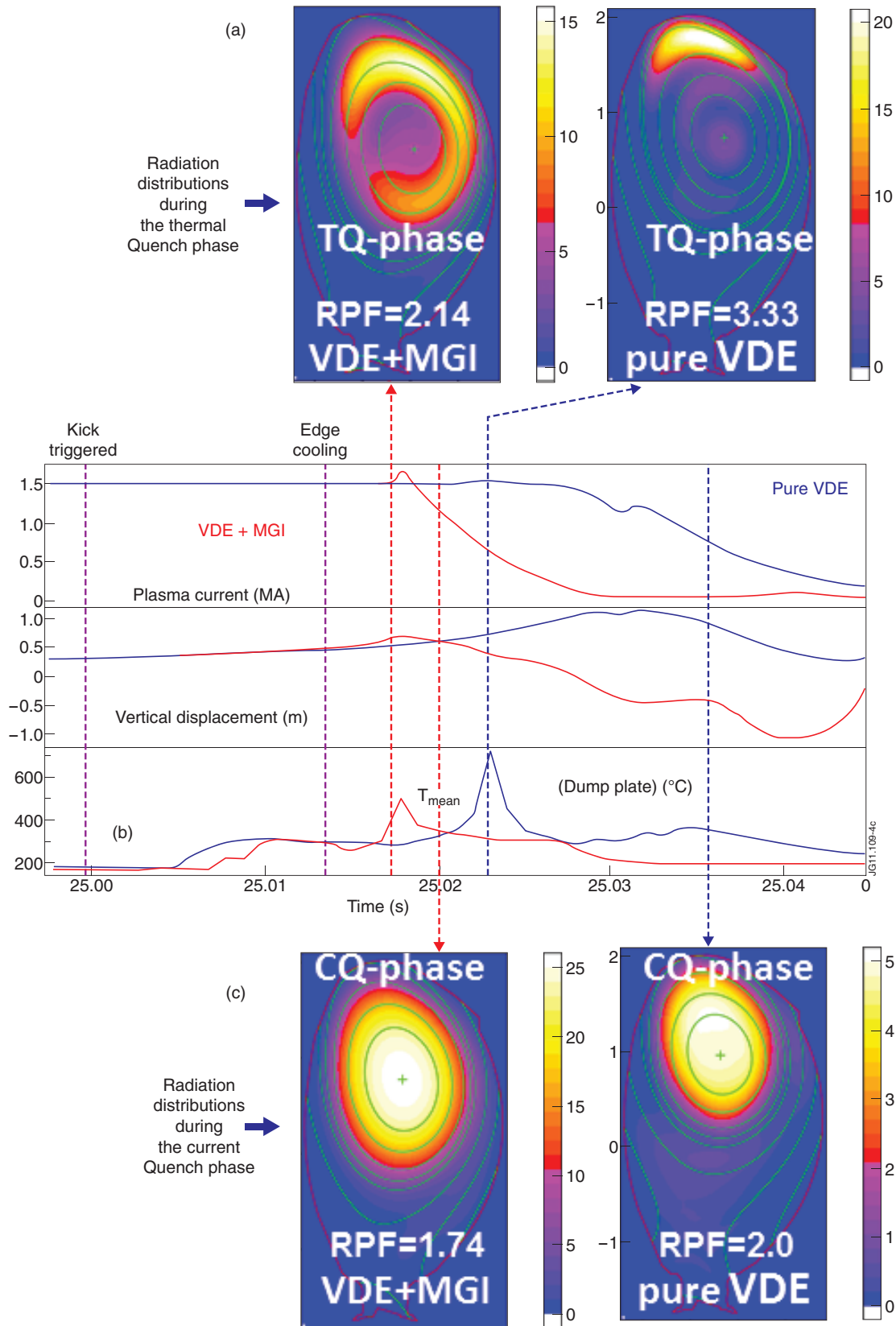


Figure 4: Comparison between a pure VDE disruption and a combined VDE + MGI experiment.